Received 4 July 2024; revised 6 September 2024; accepted 8 September 2024. Date of publication 11 September 2024; date of current version 22 November 2024.

Digital Object Identifier 10.1109/OJAP.2024.3457989

Analytical Characterization of a Transmission Loss of an Antenna-Embedded Wall

LAURI VÄHÄ-SAVO [1], LORENZO VEGGI [2], ENRICO M. VITUCCI [2] (Senior Member, IEEE), CLEMENS ICHELN [1], VITTORIO DEGLI-ESPOSTI [2] (Senior Member, IEEE), AND KATSUYUKI HANEDA [1] (Member, IEEE)

[1] Department of Electronics and Nanoengineering, School of Electrical Engineering, Aalto University, 00076 Espoo, Finland
[2] Department of Electrical, Electronic and Information Engineering "G. Marconi," CNIT, University of Bologna, 40136 Bologna, Italy

CORRESPONDING AUTHOR: L. VÄHÄ-SAVO (e-mail: lauri.vaha-savo@aalto.fi)

The work was supported by the Academy of Finland Research Project "Signal-Transmissive-Walls with Embedded Passive Antennas for Radio-Connected Low-Energy Urban Buildings (STARCLUB)," under Decision 323896.

ABSTRACT An analytical model for an antenna-embedded wall, also called *signal-transmissive wall*, is presented in this work. In the signal-transmissive wall, multiple antenna elements are distributed periodically on both wall sides, and connected back-to-back through coaxial cables. Numerical full-wave simulations of the signal-transmissive wall are computationally demanding due to the fine meshes required in the cables while having an electrically large wall size. Therefore the simulations above 8 GHz are not feasible even with a powerful cluster computer of the authors' research site. The analytical model is an attractive alternative to the full-wave simulation of the wall, which combines the individual transmission characteristics of the bare wall, realized gains of antenna elements and cable losses. The analytical model accurately reproduces the full-wave simulated transmission coefficient of the signal-transmissive wall up to 8 GHz for arbitrary polarizations and incident angles of a plane wave. The model therefore allows analysis of the signal-transmissive wall beyond 8 GHz, showing more than 70 dB reduction of the transmission loss at 30 GHz compared to a bare wall.

INDEX TERMS Antenna-embedded walls, analytical modeling, smart buildings.

I. INTRODUCTION

FUTURE generation networks promise ultra-reliable low-latency communications and enhanced mobile broadband for an even higher number of users than the legacy networks [1]. To achieve this, higher carrier frequencies are assigned to mobile communication networks from which the 3.5 GHz frequency band has already been widely adopted. The use of higher carrier frequency is more prone to greater penetration losses through materials and hence is a challenge for the indoor coverage by the outdoor base stations. Higher carrier frequencies and new energy-efficient buildings with low-emissive windows and multi-layered thermal insulations have made the operation environment extremely challenging [2], [3], [4]. The driving force to use these insulating structures is EU directives on nearly zero-energy buildings [5]. These directives have been taken as a part of national regulation in, e.g., Finland [6].

In previous works of the authors [7], [8], [9], [10] we introduced an antenna embedded wall called *a signal-transmissive wall* where passive antenna elements were embedded back-to-back to a load bearing concrete sandwich wall. Numerical full-wave simulation models of the signal-transmissive wall were verified against experiments up to 8 GHz radio frequency in [8]. However, the full-wave simulation to derive transmission coefficients of an incident plane wave was time-consuming in general because of their excessive size and multi-layered structure containing distributed electronic components. The full-wave simulation was infeasible above 8 GHz even with the best computational resource of a cluster computer in the authors' venue. We therefore present in this work an alternative approach to the full-wave simulation for more feasible analysis of the wall by developing an analytical model of the transmission coefficients through the signal-transmissive wall. The analytical model combines transmission characteristics of individual components in the signal-transmissive wall, i.e., multi-layered wall structure and the embedded antenna systems, making the calculation much lighter than the full-wave simulation of the wall. The analytical model takes the antenna radiation pattern as an input and provides estimates of the transmission coefficient through the wall at the frequency range of interest, given an incident angle and field polarization of a plane wave.

In summary, the novel contributions of the present paper are summarized in three-fold as

1) An analytical model to estimate the transmission coefficients of plane waves propagating through the signal-transmissive wall;
2) The verified effectiveness of the analytical model for different plane wave incident angles and antenna systems that reproduces the corresponding experimentally-proven full-wave numerical simulations up to 8 GHz; and finally,
3) A design of the signal-transmissive wall working up to 30 GHz using the analytical model, which would have been impossible to obtain when relying on the full-wave simulations of the wall.

The rest of the paper is organized as follows: Section II defines the signal transmissive wall and antenna system used in this paper. Also, the simulation models used to validate the analytical model are presented. Section III introduces the analytical formulation of the transmission characteristics of an incident plane wave to a normal load-bearing wall and signal-transmissive wall. The radiation or transmission characteristics of the bare wall, indoor and outdoor facing antennas, as well as coaxial cables, are defined analytically leading to a closed-form presentation of transmission losses of an antenna-embedded wall. In Section IV the analytical model is compared to the numerical solution in the case of spiral and patch antenna systems with different incident plane wave angles up to 8 GHz where the full-wave simulations are feasible. Section V extends the study to frequencies where numerical full-wave simulations are not feasible. The transmission coefficients through the spiral-antenna-based signal-transmissive wall, optimized to operate up to millimeter wave (mmWave), are studied using the developed analytical model. Section VI concludes the work.

II. SIGNAL TRANSMISSIVE WALL

The signal transmissive wall consists of multiple components like a wall, antenna elements, and coaxial cables. In this paper, we continue working on the same bare load-bearing wall, i.e., wall without embedded antenna systems, as used in our previous works [7], [8], [9], [10] as illustrated in Fig. 1(a). The wall consists of 220 mm thick mineral wool which is sandwiched between 70 and 150 mm thick concrete slabs, leading to $d_w = 440$ mm total thickness.

The signal-transmissive wall is made from back-to-back antenna systems embedded into a load-bearing wall as illustrated in Fig. 1(b). A single antenna system in the signal-transmissive wall consists of two antenna elements,

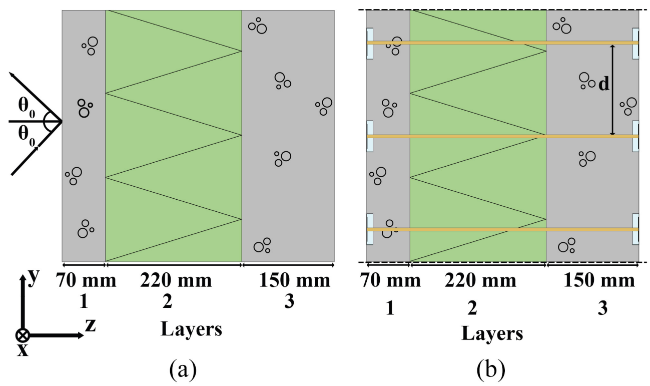

FIGURE 1. Side view of a) A bare concrete sandwich load-bearing wall. The wall is made of 70 mm-thick reinforced concrete (layer 1), 220 mm-thick rock wool for thermal insulation (layer 2), and 150 mm-thick reinforced concrete for structural bearing (layer 3). b) Signal-transmissive wall. ϕ-coordinate is from y-axis towards x-direction. The plane wave is incident at an angle of θ_0 and propagates towards the $+z$ direction.

illustrated by the light blue boxes in Fig. 1(b), connected back-to-back with a semi-rigid coaxial cable assembly. Antenna systems are embedded every $d = 150$ mm to the wall surfaces on both x and y-directions in this paper. An elementary cell of the wall refers to a piece of the wall of $d \times d \times d_{\text{wall}}$ volume, respectively on the $x \times y \times z$ dimensions, centered at the antenna system. The elementary cell is repeated around itself along the x and y axes, creating a virtually infinitely large signal-transmissive wall.

In this work, the electromagnetic fields that interact with the wall are chosen to be a plane wave, propagating in the $+z$ direction with an incident angle of θ_0. Upon incidence, part of the wave is transmitted through the wall while part is reflected. In this paper, we concentrate solely on the transmitted portion of the wave, as it is the primary focus of our analysis.

Next spiral and patch antenna systems are presented. They are used as example antenna systems and later to validate the analytical model.

A. SPIRAL ANTENNA SYSTEM

The signal-transmissive wall can be made using numerous types of antenna elements, in this paper, we use antenna elements presented in [7], [8]. The first one is a spiral antenna element, which is designed to avoid detuning effects due to concrete using a foam backing as shown in [8]. The spiral antenna elements, placed on layers 1 and 3 on the surface of the wall, are connected back-to-back by a dual-coaxial cable creating a well-matched balanced connection between the two spiral antenna elements. The spiral antenna system is shown to operate from 2.7 up to 8 GHz. The size of the numerical simulations, represented by the number of meshes, increases as the structure becomes larger compared to the wavelength when frequency increases. The numerical unit cell simulations are based on Floquet theory as explained in [8]. The electromagnetic field at any point in the unit cell can be considered a Fourier series whose basis functions are the Floquet modes [11].

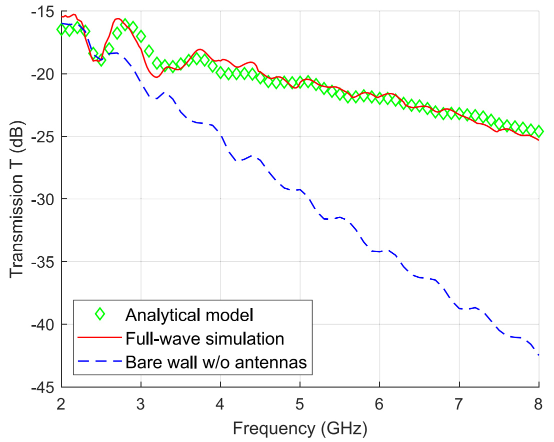

FIGURE 2. Transmission coefficients through the signal transmissive wall embedding the spiral antenna systems, compared between analytical calculation (9) and numerical simulation. Transmission coefficients through the bare wall, i.e., wall without embedded antenna systems, estimated by (4), are overlaid as a reference.

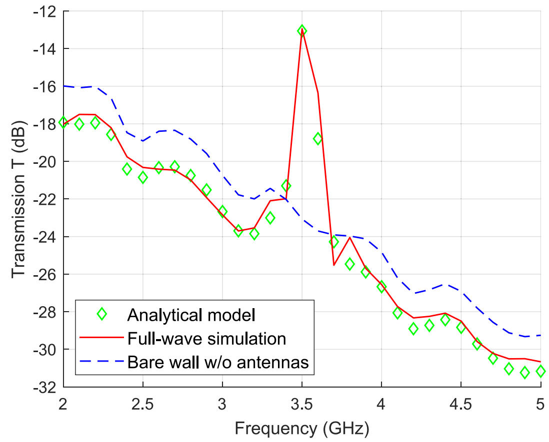

FIGURE 3. Transmission coefficients through patch antenna system embedded to a load bearing wall, compared between the analytical calculation (9) and numerical simulation. Transmission coefficients through a bare wall, i.e., wall without embedded antenna systems, estimated by (4), are overlaid as a reference.

Unlike in waveguides, the group velocities of Floquet modes are constant but the phase velocities are not. As the frequency increases the number of propagating Floquet modes increases, leading to a greater number of non-zero elements in matrices formulated by the finite element methods and hence increased memory consumption. For the elementary cell size of $d = 150$ mm, the number of propagating Floquet modes is between 100 and 400 modes at 8 GHz depending on the incident angle. Because of the computational limitations, it is not possible to simulate the spiral antenna system above 8 GHz. Figure 2 shows full-wave simulated transmission through the signal-transmissive wall. We aim to reproduce the transmission curve from full-wave simulations with the analytical calculation, which is covered in the next section. This spiral antenna system was empirically validated in [8].

B. PATCH ANTENNA SYSTEM

The second antenna system is the patch antenna system presented in [7], where two patch antennas are connected back-to-back by a single coaxial cable. The patch antenna system operates effectively over a very narrow bandwidth. This limitation makes it less suitable for use in antenna-embedded walls, but it serves as an ideal candidate for validating our analytical model due to its different operating principle compared to the spiral antenna. Unlike the spiral antenna, the patch antenna includes a ground plane, which further differentiates the two designs. Using these two quite different antenna systems helps demonstrate the general applicability of the analytical model.

To satisfy thermal insulation regulations set by the Finnish government [6], the size of the cable is reduced, and the conductor material is changed to stainless steel compared to the original design in [7]. The coaxial cable center conductor diameter is 0.92 mm, the dielectric diameter is 3.17 mm, and the thickness of the shield is 0.2 mm. The antenna system is designed to resonate at 3.5GHz. Figure3 shows the transmission coefficients through the wall with the patch antenna system. As with the spiral antenna system, we model the numerically simulated transmission coefficients analytically.

III. ANALYTICAL MODEL

In this section, all the components of the signal-transmissive wall are defined analytically. Several different approaches have been used to estimate the electromagnetic transmission through a building wall. These methods can be divided into closed- and open-form solutions. Closed-form solutions include plane-wave-based methods like the ones in [12], [13]. Open-form solutions are derived from the method-of-moments (MoM), cylindrical wave approaches, finite-element method (FEM), and combining Green's functions to those [14], [15], [16], [17], [18]. Our choice is to use a closed-form formulation to describe the transmission through an antenna-embedded wall because of its computational efficacy and insight into the operation of individual components in the signal-transmissive wall.

A. TRANSMISSION THROUGH BARE WALL

ITU-R P.2040 [12] defines the complex relative permittivities of most common building materials above 100 MHz as

$$\epsilon_{\mathrm{r}}(f) = \epsilon' - j\epsilon'' = af^b - j\frac{cf^d}{\epsilon_0\omega}, \tag{1}$$

where the a, b, c and d determine the frequency dependent permittivity while f is the frequency in GHz and ω is the angular frequency in radians. Transmission through the bare wall can be calculated using the iterative method that takes into account the multiple reflections inside the wall presented in [13] Section V-D.5 as

$$A_n = 0.5 \cdot \exp(\mathrm{j}k_n d_n \cos\theta_n) \big[A_{n+1}(1 + Y_{n+1}) + B_{n+1}(1 - Y_{n+1})\big], \tag{2}$$

$$F_n = 0.5 \cdot \exp(\mathrm{j}k_n d_n \cos\theta_n) \big[F_{n+1}(1 + W_{n+1}) + G_{n+1}(1 - W_{n+1})\big], \tag{3}$$

where $0 \leq n \leq N$ is an index of a dielectric layer and N is the total number of dielectric layers, $A_{N+1} = 1$, $F_{N+1} = 1$ and $W_{n+1} = \frac{\cos\theta_{n+1}}{\cos\theta_n}\sqrt{\frac{\epsilon_n}{\epsilon_{n+1}}}$, $Y_{n+1} = \frac{\cos\theta_{n+1}}{\cos\theta_n}\sqrt{\frac{\epsilon_{n+1}}{\epsilon_n}}$ and $\sin\theta_n = \frac{\sin\theta_0}{\sqrt{\epsilon_n}}$ representing Snell's law, $k_n = \frac{2\pi}{\lambda}\sqrt{\epsilon_n}$ is the wavenumber in the dielectric, λ is the wavelength in free space in meters and θ_0 is the plane wave incident angle in degrees defined in Fig. 1(b). Now the transmission coefficient can be written as

$$T_{\mathrm{TE}} = \frac{1}{A_0} \text{ and } T_{\mathrm{TM}} = \frac{1}{F_0} \tag{4}$$

where TE and TM refer to transverse-electric and transverse-magnetic incident polarization respectively. To define circular or elliptical polarization we need to combine both linear polarizations with the appropriate weight, leading to a transmission coefficient T_{wall}; finally, the loss of an electromagnetic field through a bare wall with any polarization is given by $L_{\mathrm{wall}} = 1/|T_{\mathrm{wall}}|^2$.

B. POWER LOSSES THROUGH THE SIGNAL-TRANSMISSIVE WALL

Antennas cover only a portion of the load-bearing wall surface meaning that some of the power is captured by the antenna system and some is going through the wall. To account for this effect in the analytical model we define the efficiency parameter η_{phy} to represent a portion of the wall covered by the antennas as

$$\eta_{\mathrm{phy}} = \frac{A_{\mathrm{ant}}}{A_{\mathrm{cell}}} \tag{5}$$

where A_{ant} is the size of the metallization of the antenna and $A_{\mathrm{cell}} = d^2$ is the area of the elementary cell of the wall. The physical size of an antenna element, which is identical to its metallization area A_{ant}, needs to be considered since it blocks part of the incident plane wave. Then, $(1 - \eta_{\mathrm{phy}})^2$ is the portion of incident power density that goes through the bare wall.

The antenna's capability to capture the power density from the incident plane wave is defined by the effective aperture of the antenna element. On the other hand, the portion of the incident power captured by the antenna in the center of the elementary cell, including the effect of losses and mismatches, can be defined as

$$\eta_{\mathrm{eff}} = \frac{A_{\mathrm{eff}}}{A_{\mathrm{cell}}} = \frac{\lambda^2}{4\pi} G_{\mathrm{re}} \cdot \frac{1}{A_{\mathrm{cell}}}, \tag{6}$$

where G_{re} is the realized gain of the antenna towards the direction of the incident plane wave at the frequency of interest. The realized gain of the antenna element can be defined either analytically, from numerical simulations, or measurements. In this work, we use numerical full-wave simulations made with CST studio to obtain the realized gain patterns. Accurate characterization of weak gain levels is usually more challenging than stronger levels. As weaker gains of antennas are observed for higher radio frequencies and larger radiation angles off the normal direction, their numerical simulations need special attention. For example, adaptive mesh refinement was used and the maximum energy level at the end of the simulation was set to −60 dB. It is important that we use η_{eff} and not η_{phy} to model the antenna elements since the power density arriving at the antenna's physical aperture is not only captured by the antenna but also reflected on the metallic ground plane.

C. COAXIAL CABLE ATTENUATION

The next component in the back-to-back antenna system is the coaxial cable. Attenuation in a coaxial cable is mainly caused by the skin effect on metals and secondarily by ohmic losses on the dielectric. In this study, different metals must be considered for the shield and center conductor in order to reduce the electromagnetic losses through the antenna system while maintaining the required thermal insulation. This choice of metal in cables led to the analytical formula of electromagnetic losses in Neper per meter as [9]

$$\alpha = \alpha_c + \alpha_d = \frac{1}{2\mathbb{R}[\eta_{\mathrm{d}}]}\left(\frac{R_{\mathrm{s_i}}}{r_{\mathrm{i}}} + \frac{R_{\mathrm{s_o}}}{r_{\mathrm{o}}}\right)\frac{1}{\ln\frac{r_{\mathrm{o}}}{r_{\mathrm{i}}}} + \frac{\omega}{2c}\tan_{\delta}, \tag{7}$$

where α_c and α_d are attenuation coefficients in conductors and in the dielectric; $R_{\mathrm{s_i}}$ and $R_{\mathrm{s_o}}$ are the sheet resistances of the conductors and r_{i}, r_{o} are the radius of the center conductor and shield, respectively; η_d is the impedance of the dielectric; c is the speed of light in the dielectric; $\tan_\delta$ is the loss tangent of the dielectric. Eq. (7) is similar to [19, eq. (11).4.9], but suitably extended to the case of a coaxial cable with center and shield conductors made of different materials, according to the procedure explained in [9]. Multiplying the conversion factor 8.686 from a linear to decibel scale, the total attenuation in dB of the coaxial cable assembly is $\alpha_{\mathrm{dB}} = 8.686 \cdot \alpha \cdot d_{coax}$.

D. RE-RADIATING ANTENNA ELEMENT

Finally, the antenna on the re-radiating side of the back-to-back antenna systems is modeled. Since we are interested in the total power transmitted to the other side of the wall, the re-radiating antenna is modeled with its total efficiency, ϵ_{tot}, towards the half sphere away from the wall. It is calculated from the radiation pattern over the solid angle Ω of 2π, which represents the ratio of radiated power to the half sphere and input power. This allows us to define the antenna system loss $L_{\mathrm{ant}} = 10^{\frac{\alpha_{\mathrm{dB}}}{10}} \cdot \epsilon_{\mathrm{tot}}$.

E. ANALYTICAL MODEL OF TRANSMISSION COEFFICIENTS FOR THE SIGNAL-TRANSMISSIVE WALL

Now all the components of the signal transmissive wall are defined and we can combine the analytical model as

$$T|_{\mathrm{dB}} = 10\log_{10}\left(\frac{\eta_{\mathrm{eff}}}{L_{\mathrm{ant}}} + \frac{(1 - 1.7\eta_{\mathrm{phy}})^2}{L_{\mathrm{wall}}}\right) \tag{8}$$

$$= 10\log_{10}\left(\frac{\frac{\lambda^2}{4\pi}G_{\mathrm{re}} \cdot \frac{1}{A_{\mathrm{cell}}}}{10^{\frac{\alpha_{\mathrm{dB}}}{10}} \cdot \epsilon_{\mathrm{tot}}} + \left(1 - 1.7\frac{A_{\mathrm{ant}}}{A_{\mathrm{cell}}}\right)^2 |T_{\mathrm{wall}}|^2\right). \tag{9}$$

The model is made from two parts, one representing the effects of the antenna system and the other representing the effects of the wall. Both parts have a portion of incident power in the numerator and losses in the denominator. It must be noted that η_{phy}, representing the physical antenna size, is multiplied with a heuristic factor of 1.7 in (9) since an incident plane wave is blocked by antennas with a metallic ground plane on layers 1 and 3. Even for a plane wave incident normal to the wall, scattered fields inside the wall are subject to the blockage due to the re-radiating antennas, leading to the multiplied coefficient.

IV. VALIDATION OF THE ANALYTICAL MODEL

In this Section, the accuracy of the analytical model is shown in the case of normal and grazing incidence of a plane wave to the wall. Also, the transmission coefficient of the signal transmissive wall with the spiral antenna system is shown up to mmWave bands. Most of the presented results are compared against numerical simulations detailed in [8] to show the accuracy of the analytical model.

A. PLANE WAVE WITH NORMAL INCIDENCE

Figure 2 shows a comparison of transmission coefficients through the signal-transmissive wall with the spiral antenna system, calculated with the analytical model and a numerical simulation. The analytical calculation agrees well with the numerical simulation, justifying the developed analytical model in Section III. There are some small differences in the transmission curves which can be caused by differences in numerical simulation accuracy when antennas are simulated as a separate entity or as a part of the wall. The analytically calculated and numerically simulated transmission coefficients have an average difference of 0.072 dB, where the negative value means that the analytically calculated transmission coefficient is greater. The standard deviation was 0.57 dB over the frequency range of 2 to 8 GHz.

Transmission through the signal-transmissive wall composed of patch antenna systems is shown in Fig. 3. The analytical model gives the transmission coefficient derived from full-wave simulation accurately across the frequencies. At off-band, the inclusion of the antenna systems led to 1.9 dB higher losses of the incident plane wave because the antenna system blocks radiation due to the metalized ground plane. Similarly, as with the spiral antenna system, we see small differences between the analytically-derived and full-wave simulated coefficients, e.g., at 3.6 and 3.8 GHz, partly due to the missing mutual coupling effect when deriving the radiation patterns. The transmission coefficients calculated with the analytical model and numerical simulations have an average difference of -0.29 dB with a standard deviation of 0.63 dB across the frequency from 2 to 5 GHz.

B. PLANE WAVE WITH GRAZING INCIDENCE

The analytical model must be capable of estimating transmission coefficients through the wall with an arbitrary

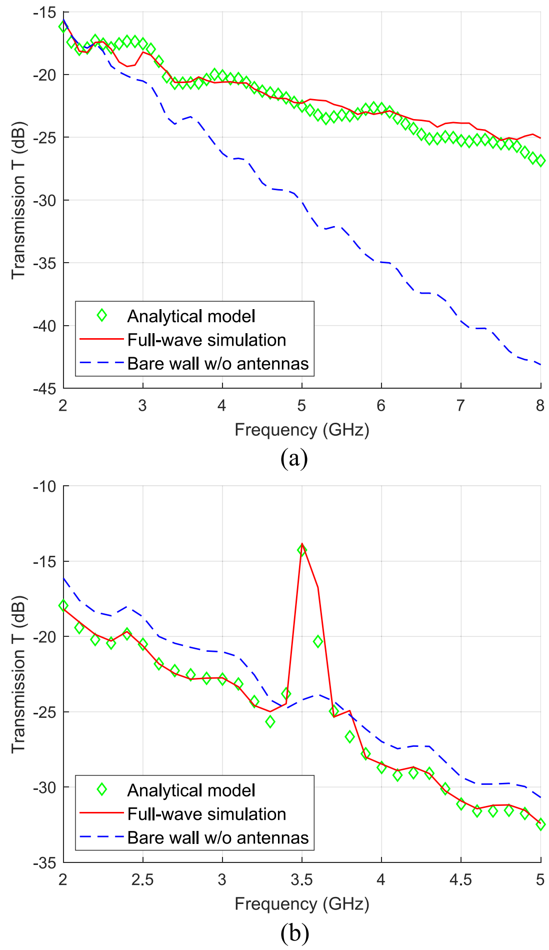

FIGURE 4. Transmission coefficients through the signal-transmissive wall with (a) spiral and (b) patch antenna element, with 30° plane wave incident angle, compared between the analytical calculation Eq. (9) and numerical simulation. The coefficients for the bare wall, i.e., wall without embedded antenna systems, are also derived from Eq. (4) with 30° plane wave incidence.

incidence angle of a plane wave. To test this we performed numerical simulations with the spiral antenna system with $\theta = 30^\circ$ incident angles to obtain the transmission coefficient using full-wave simulations and then to compare them with the analytical calculation. Note that we here use the identical radiation patterns of the spiral antenna as those calculated for the normal incidence of the plane wave. Figure 4(a) shows a comparison of the transmission coefficients through the signal-transmissive wall with the spiral antenna element calculated with the analytical model and numerical simulation, showing good agreement above 3GHz. Around 2.7 GHz, where the antenna starts to operate, the analytical model overestimates the transmission by up to 2 dB. Figure 4(b) shows the transmission coefficients through the signal-transmissive wall with the patch antenna element calculated with the analytical model and numerical simulation; $30^{c}irc$ plane wave incident angle is assumed. The figure shows good agreement throughout the band.

The full-wave simulations of a signal-transmissive wall are more time-consuming and hence infeasible because the greater angle of the incident plane wave leads to the increasing number of propagating Floquet modes. While the analytical model considers various incident plane wave angles by a radiation pattern of a *single* antenna element. Therefore the analytical model has a significant advantage in calculating the transmission coefficient of off-normal plane wave incidence on the signal-transmissive wall compared to the full-wave simulation of the same.

V. THE SPIRAL ANTENNA SYSTEM AT MMWAVE BAND

Finally, using the analytical model, the signal-transmissive wall can be designed for the antenna separation distance d and materials of the coaxial cables, at frequencies that cannot be studied using numerical simulation software due to the excessive computational time required. Even with the best computational resource of a cluster computer in the authors' venue, numerical transmission simulations above 8 GHz are not feasible with an elementary cell size of 150×150 mm^2. While the radiation patterns of a *single* antenna element on top of the concrete slab can be simulated even at the mmWave frequencies, which can be incorporated into the analytical model to derive the transmission coefficients of the signal-transmissive wall at the mmWave.

A. IMPROVED SPIRAL ANTENNA ELEMENT

The spiral antenna was optimized only up to 8 GHz in [8]. Now we need to improve the antenna system to extend the bandwidth up to mmWaves. First, the feed gap of the antenna allowed good impedance matching only up to 12 GHz. Therefore, triangular matching elements are added to both legs of the spiral antenna to improve impedance matching over the whole frequency band. Secondly, a coaxial cable with a smaller dimension, which has a center pin with 0.143 mm diameter and an outer connector with 0.875 mm diameter with 0.1 mm thickness, is introduced. Third, the dielectric of the coaxial cable is now low-density PTFE with relative permittivity of 1.75 and loss tangent of 0.0002. Finally, the foam backing of the antenna shape was changed to be half ellipsoid with $22 \times 22 \times 8.5$ mm^3 dimension along the $x \times y \times z$ axes. Compared to using rectangular form backing of the antenna in [8], the use of the half ellipsoid backing saves more space for the concrete parts of the load-bearing wall by 31 %. Figure 5 shows the improved structure of the spiral antenna.

The realized gains and total efficiency of the improved antenna is simulated up to 30 GHz for the analytical model. Figure 6 shows the maximum of the realized gain on the front hemisphere, realized gain towards the normal direction, and total efficiency on the front hemisphere of the antenna. As can be seen, both the realized gain and total efficiency drop drastically between 15 and 19 GHz. Above 19 GHz the maximum realized gain starts to increase and the total efficiency toward the front hemisphere stabilizes around −6.3 dB. Realized gain towards the normal direction shows two dips at 18 and $\sim$ 30 GHz. These dips are caused by destructive interference resulting from reflections between the antenna element and the layer of concrete behind the antenna. By adjusting, e.g., the depth of the foam cavity behind the antenna, the dips in realized gain can be shifted to other frequencies, if necessary. Figure 7 shows $\phi = 0°$ and $\phi = 90°$ cuts of the radiation pattern of the spiral antenna at 5, 10, 15, 20, 25 and 30 GHz. The realized gain patterns below 15 GHz are smooth. At 20 GHz, the pattern exhibits lower gain due to multiple reflections between the antenna and the concrete. At 25 GHz, the maximum gain is approximately 6 dBi, but the 3−dB beamwidth is reduced to just 30°, which explains the lower total efficiency observed in Fig. 6. At 30 GHz, the pattern becomes deformed, with two side lobes starting to dominate the radiation pattern. This deformation is caused by reflections between the antenna and the concrete, leading to destructive interference.

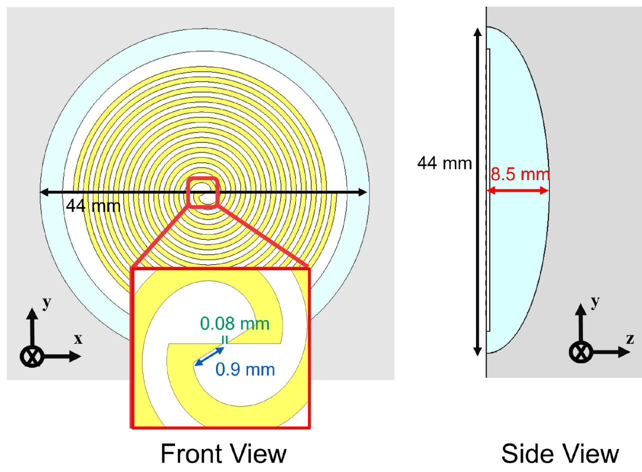

FIGURE 5. Dimensions of the improved spiral antenna element that expands the impedance matching up to 30 GHz. The gray color is concrete, light blue is foam, white is PCB, and yellow is copper.

B. IMPROVED COAXIAL CABLES

Improvement has also been made to the coaxial cable connecting two back-to-back spiral antennas according to the results presented in [9]. The center conductor material on coaxial cables is changed from stainless steel in [8] and Section III-E to beryllium copper which leads to lower attenuation in a coaxial cable. The same antenna separation of $d = 150$ mm which meets the limit of thermal transmittance given in the national building regulation [6] while the coupling between antenna elements is negligible at the lowest frequencies of 2.7 GHz.

C. REALIZED TRANSMISSION CHARACTERISTICS

Figure 8 shows the transmission coefficients through the signal-transmissive wall with improved spiral antennas from 2 to 30 GHz for the normal incident angle, which was estimated using (9). The transmission drops from −24.7 to −45 dB between 10 and 18.5 GHz but then increases to −37 dB and stays above −40 dB up to 27.5 GHz covering the whole NR-FR2 n258 band. At the n258 band, the transmission through the bare wall is less than −100 dB according

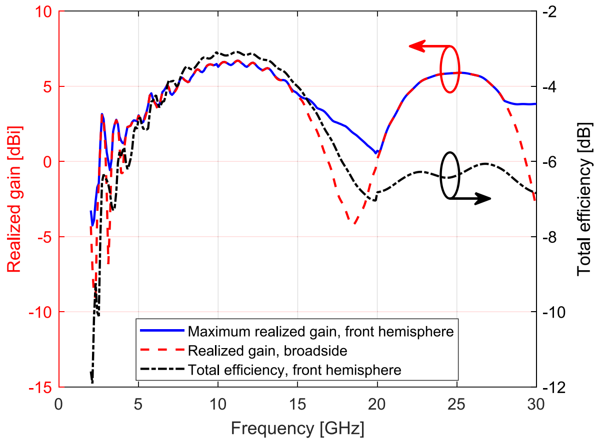

FIGURE 6. The realized gain and total efficiency of the improved spiral antenna element from 2 to 30 GHz.

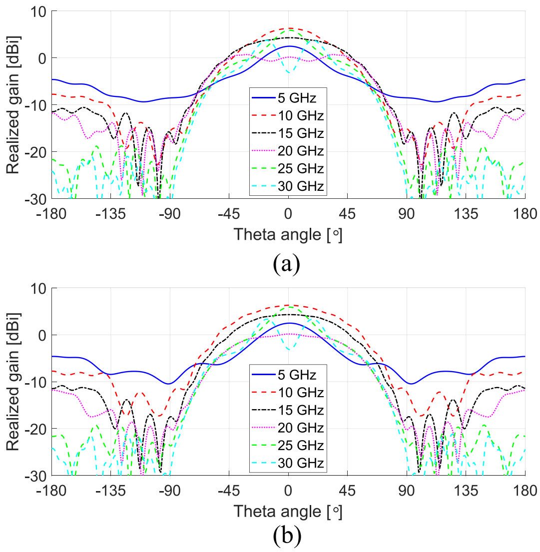

FIGURE 7. Radiation pattern cuts of the improved spiral antennas a) $\phi = 0^\circ$ and b) $\phi = 90^\circ$ at 5, 10, 15, 20, 25 and 30 GHz.

to (4), leading to 73.4 dB improvement at 27.5 GHz. Transmission coefficients through the signal-transmissive wall with the improved spiral antenna system were also simulated up to 8 GHz. The average difference between analytical calculation and numerical full-wave simulations is -0.57 dB with a standard deviation of 0.8 dB.

VI. CONCLUSION

In this study, we have presented an analytical approach to estimate the electromagnetic transmission coefficient through the signal-transmissive wall. The analytical model was accurate with arbitrary polarizations and incidence angles of a plane wave for both spiral and patch antenna elements. Finally, the analytical model was used to estimate the transmission coefficients through the signal-transmissive wall at mmWave frequencies, which the sole full-wave simulations could not solve due to computationally prohibitive electrically large structures. More than 70 dB reduction of

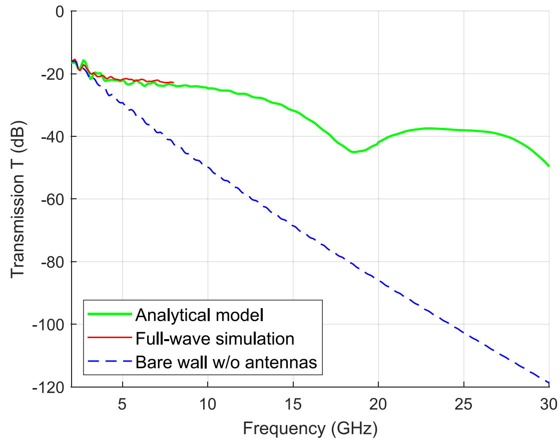

FIGURE 8. Transmission coefficients of a normally incident plane wave to the signal transmissive wall and the bare wall, i.e., wall without embedded antenna systems, estimated with the analytical models (4) and (9), respectively. Numerically simulated transmission coefficient between 2 and 8 GHz as a reference.

the transmission loss was achieved compared to the bare wall at NR-FR2 n258 band, giving 40 dB maximum loss in the band. Despite the significant reduction of the loss compared to the bare wall, the 40 dB loss may still be too high from a radio link design perspective. An improved antenna system design with probably amplifiers integrated as a part of the antenna system might be needed to support mmWave, which we cannot simulate numerically but only with our analytical model. Combined with the analytical *thermal* transmission model presented in [9], our analytical model is a powerful multi-physics tool allowing electromagnetic and thermal insulation analysis for designing antenna-embedded walls.

REFERENCES

[1] *IMT Vision—Framework and Overall Objectives of the Future Development of IMT for 2020 and Beyond*, ITU-Rec. M.2083-0, Int. Telecommun. Union, Geneva, Switzerland, Sep. 2015. [Online]. Available: https://www.itu.int/dms_pubrec/itu-r/rec/m/R-REC-M.2083-0-201509-I!!PDF-E.pdf

[2] I. Rodriguez, H. C. Nguyen, N. T. K. Jorgensen, T. B. Sorensen, and P. Mogensen, "Radio propagation into modern buildings: Attenuation measurements in the range from 800 MHz to 18 GHz," in *Proc. IEEE 80th Veh. Tech. Conf.*, 2014, pp. 1–5.

[3] P. Koivumäki, A. Karttunen, and K. Haneda, "Ray-optics simulations of outdoor-to-indoor multipath channels at 4 and 14 GHz," *IEEE Trans. Antennas Propag.*, vol. 71, no. 7, pp. 6046–6059, Jul. 2023.

[4] L. Van der Perre, E. G. Larsson, F. Tufvesson, L. D. Strycker, E. Björnson, and O. Edfors, "RadioWaves for efficient connectivity: Analysis and impact of constraints in actual deployments," in *Proc. 53rd Asilomar Conf. Signals, Syst., Comput.*, 2019, pp. 15–22.

[5] (Eur. Comm., Brussels, Belgium). *European Union Directive on Nearly Zero-Energy Buildings*, 2019. [Online]. Available: https://energy.ec.europa.eu/topics/energy-efficiency/energy-efficient-buildings/nearly-zero-energy-buildings_en

[6] (Minist. Environ. Finland, Helsinki, Finland). *1010/2017 Decree of the Ministry of the Environment on the Energy Performance of New Buildings*. Dec. 2017. [Online]. Available: https://ym.fi/en/the-national-building-code-of-finland

[7] L. Vähä-Savo et al., "Passive antenna systems embedded into a load bearing wall for improved radio transparency," in *Proc. Proc. 50th Eur. Microw. Conf. (EuMC)*, 2021, pp. 424–427.

[8] L. Vähä-Savo, K. Haneda, C. Icheln, and X. Lü, "Electromagnetic–thermal analyses of distributed antennas embedded into a load-bearing wall," *IEEE Trans. Antennas Propag.*, vol. 71, no. 8, pp. 6849–6858, Aug. 2023.

[9] L. Veggi, L. Vähä-Savo, K. Haneda, E. M. Vitucci, and V. Degli-Esposti, "Electromagnetic and thermal analysis of coaxial cable connection embedded in an intelligent wall," in *Proc. 17th Eur. Conf. Antennas Propag. (EuCAP)*, 2023, pp. 1–5.

[10] T. Lu, L. Vähä-Savo, X. Lü, and K. Haneda, "Thermal impact of 5G antenna systems in sandwich walls," *Energies*, vol. 16, no. 6, p. 2657, 2023. [Online]. Available: https://www.mdpi.com/1996-1073/16/6/2657

[11] S. Tretyakov, *Analytical Modeling in Applied Electromagnetics*. Norwood, MA, USA: Artech House, 2003.

[12] *Effects of Building Materials and Structures on Radiowave Propagation Above About 100 MHz*, ITU-Rec. P.2040-3, Int. Telecommun. Union, Geneva, Switzerland, Aug. 2023. [Online]. Available: https://www.itu.int/rec/R-REC-P.2040-3-202308-I/en

[13] C. A. Balanis, *Advanced Engineering Electromagnetics*, 2nd ed. Hoboken, NJ, USA: Wiley, 2012.

[14] R. Paknys, "Reflection and transmission by reinforced concrete—Numerical and asymptotic analysis," *IEEE Trans. Antennas Propag.*, vol. 51, no. 10, pp. 2852–2861, Oct. 2003.

[15] E. Richalot, M. Bonilla, M.-F. Wong, V. Fouad-Hanna, H. Baudrand, and J. Wiart, "Electromagnetic propagation into reinforced-concrete walls," *IEEE Trans. Microw. Theory Techn.*, vol. 48, no. 3, pp. 357–366, Mar. 2000.

[16] A. Torabi and A. A. Shishegar, "An accurate derivation of spatial green's function for finite dielectric structures using characteristic green's function-perfectly matched layer method," *IEEE Trans. Antennas Propag.*, vol. 62, no. 6, pp. 3201–3211, Jun. 2014.

[17] A. Parsa and C. Caloz, "Reflection characteristics of two parallel reinforced concrete slabs," in *Proc. 3rd Eur. Conf. Antennas Propag.*, 2009, pp. 2296–2299.

[18] A. Torabi and A. A. Shishegar, "Scattering with reinforced concrete wall in 900 MHz band using MOM/CI method," in *Proc. 3rd Eur. Conf. Antennas Propag.*, 2009, pp. 121–125.

[19] S. J. Orfanidis, *Electromagnetic Waves and Antennas*. 2016. [Online]. Available: https://books.google.it/books?id=4n5ezQEACAAJ